Supporting Information for Design Principles for Aqueous Na-ion Battery Cathodes

Xingyu Guo,[†] Zhenbin Wang,[‡] Zhi Deng,[‡] Bo Wang,[¶] Xi Chen,[¶] and Shyue Ping Ong[*,‡]

†*Materials Science and Engineering Program, University of California San Diego, 9500 Gilman Dr, Mail Code 0448, La Jolla, CA 92093-0448, United States*

‡*Department of NanoEngineering, University of California San Diego, 9500 Gilman Dr, Mail Code 0448, La Jolla, CA 92093-0448, United States*

¶*GEIRI North America, San Jose, CA 95134, USA*

E-mail: ongsp@eng.ucsd.edu

Calculated binary phase diagrams of all compounds

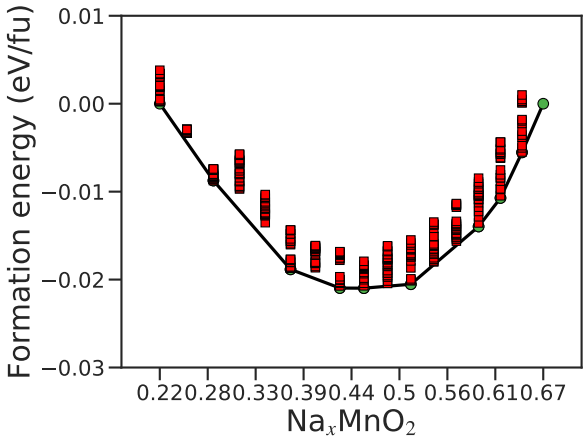

(a) Convex hull of Na_xMnO_2

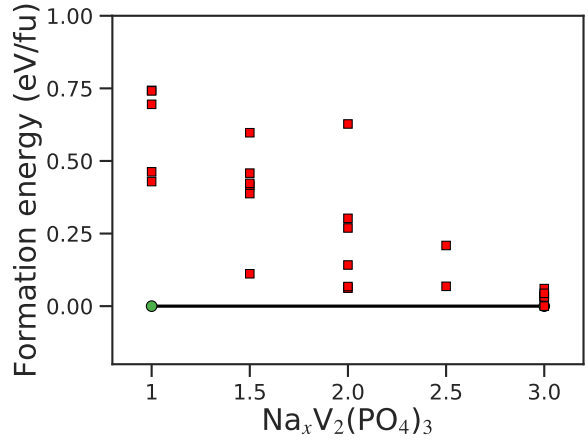

(b) Convex hull of $Na_xV_2(PO_4)_3$

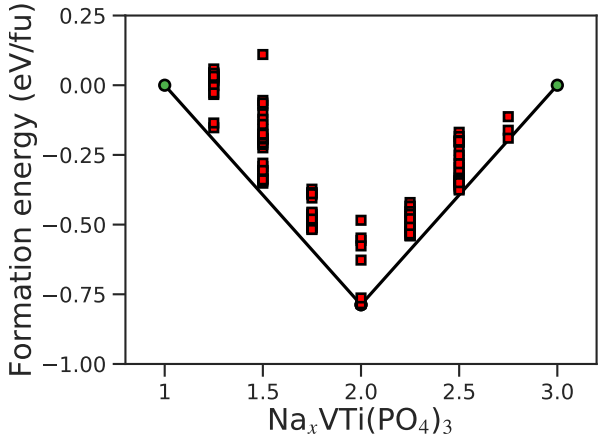

(c) Convex hull of $Na_xVTi(PO_4)_3$

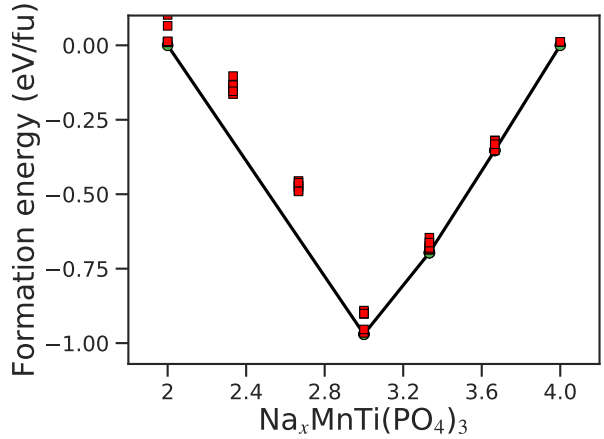

(d) Convex hull of $Na_xMnTi(PO_4)_3$

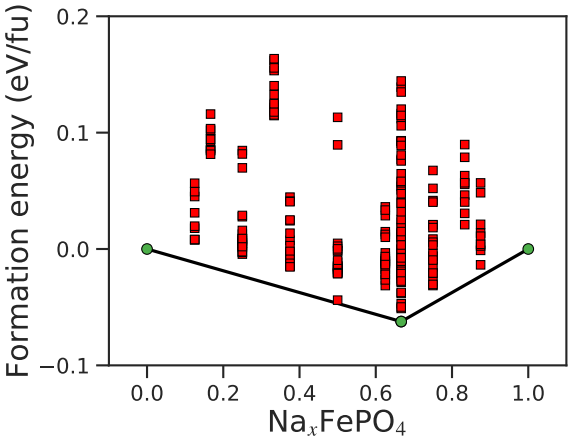

(e) Convex hull of Na_xFePO_4

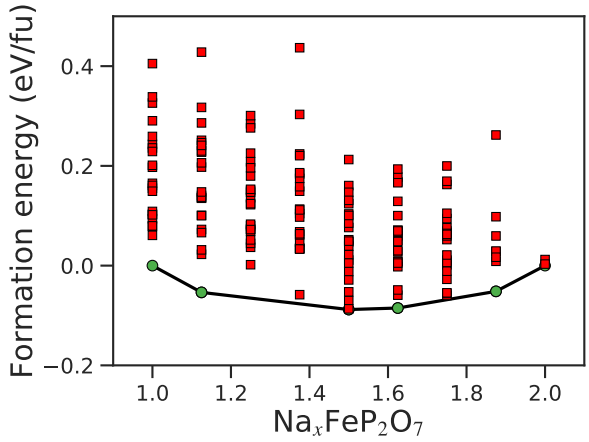

(f) Convex hull of $Na_xFeP_2O_7$

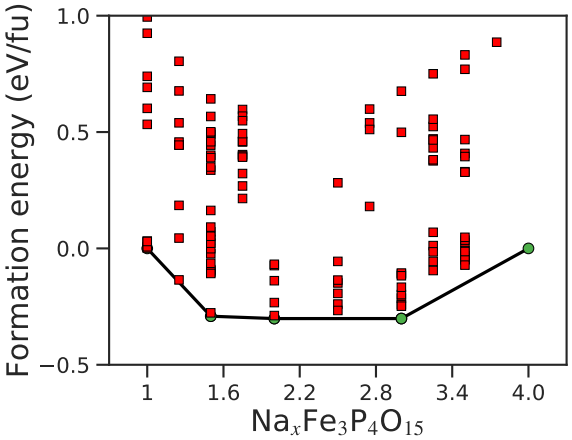

(g) Convex hull of $Na_xFe_3P_4O_{15}$

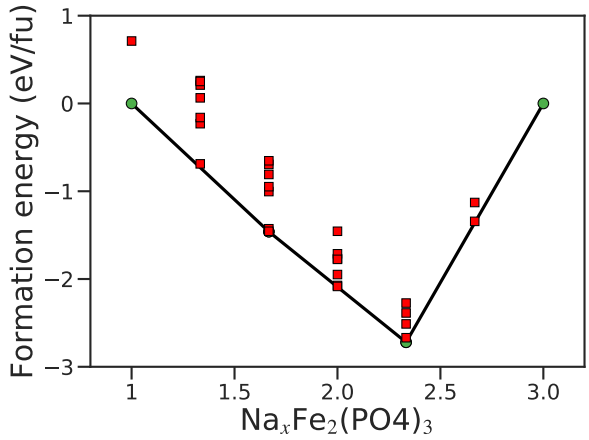

(h) Convex hull of $Na_xFe_2(PO_4)_3$

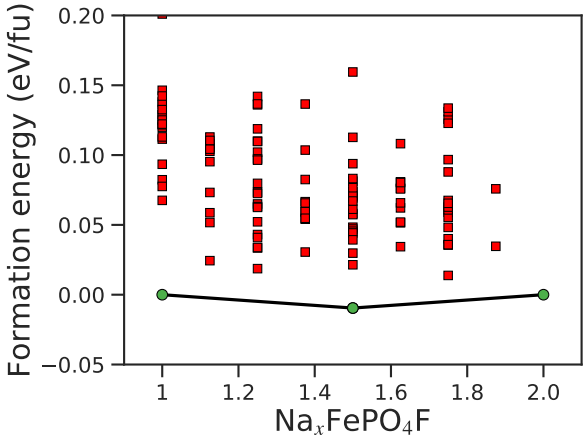

(i) Convex hull of Na_xFePO_4F

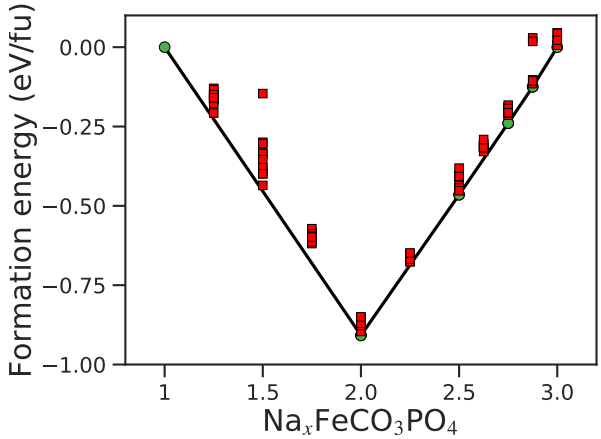

(j) Convex hull of $Na_xFeCO_3PO_4$

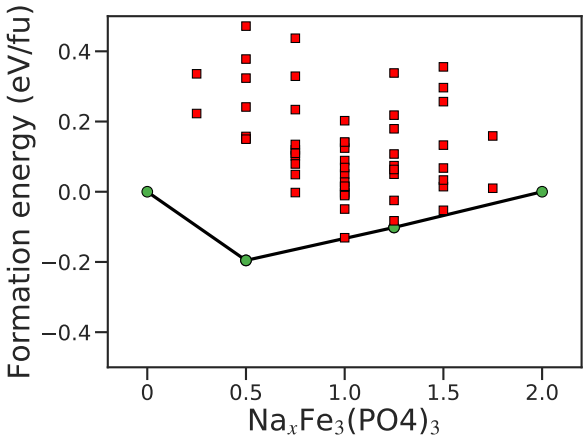

(k) Convex hull of $Na_xFe_3(PO_4)_3$

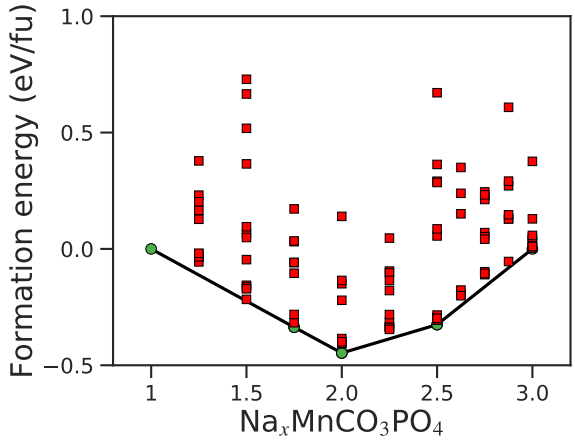

(l) Convex hull of $Na_xMnCO_3PO_4$

Figure S1: Calculated convex hull

Notes on the calculated convex hulls and voltage profiles

$Na_{0.44}MnO_2$. In experiment, there are at least six intermediate phases identified for $Na_{0.44}MnO_2$ during charge/discharge processes.[1] In our calculations, we predicted eight intermediate stable phases within the composition range of $Na_{0.22}MnO_2 \sim Na_{0.66}MnO_2$. Similarly, Kim et al.[2] reported six calculated intermediate stable phases within the same composition range. Our calculated voltage profile is consistent with the experimental results. (Figure 3(a))

$Na_3V_2(PO_4)_3$. NASICON-type $Na_3V_2(PO_4)_3$ was reported to exhibit reversible phase transition from $NaV_2(PO_4)_3$ to $Na_3V_2(PO_4)_3$ during charge/discharge processes with a single voltage plateau at 3.39 V vs Na/Na^+.[3] According to our calculated convex hull, no stable intermediate phase is found between $NaV_2(PO_4)_3$ and $Na_3V_2(PO_4)_3$, which is also in line with the computational results by Lim et al.[4].

$Na_2FeP_2O_7$. *Ex situ* XRD characterization indicates that $Na_2FeP_2O_7$ undergoes successive biphasic transitions via various intermediate phases.[5] Four voltage plateaus located at 2.52, 2.99, 3.08 and 3.24 V vs Na/Na^+ have been observed in experiments. Our calculations showed that four intermediate stable phases with respect to $Na_2FeP_2O_7$ and $NaFeP_2O_7$ and the calculated voltage profile shows five plateaus at 2.405, 2.694, 2.793, 2.910 and 3.247V vs Na/Na^+, which are close to the experimental results. The only difference is that the experimental capacity drops rapidly when the voltage is lower than 2.99 V vs Na/Na^+. Previous calculations by Kim et al.[5] also suggested four intermediate stable phases but with slightly different compositions.

$NaFePO_4$. In our calculation, there is a stable phase at $Na_{2/3}FePO_4$, which is in line with the previous experimental[6] and calculation results.[7] The calculated voltage profiles show two plateaus at 3.0 V and 2.73 V vs Na/Na^+, which is close to the voltages reported experimentally.[8]

Na_2FePO_4F. Li et al.[9] have shown that Na_2FePO_4F exhibits two two-phase reactions and form $Na_{1.5}FePO_4F$ intermediate phase at low C rate (0.1 C $\sim$ 1 C). In our calculations, we

predicted there is only one stable phase at $Na_{1.5}FePO_4F$, which is in line with experimental[9] and the computational results.[10] The calculated voltage profile shows two plateau at 2.87 and 2.91 V vs Na/Na^+, which is close to the experimental results of 2.91 and 3.06 V vs Na/Na^+.[9]

Calculated voltage profile of Na_xMnO_2 in basic electrolyte

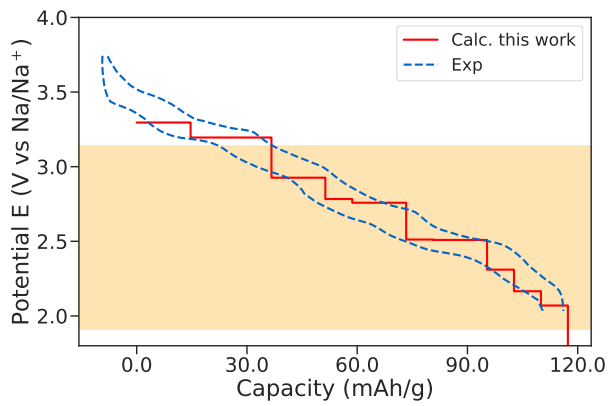

Figure S2: Calculated voltage profile of Na_xMnO_2 ($x = 0.22 - 0.66$). The electrochemical stability windows at pH = 13.5 are shaded orange. The experimental voltage profile is from ref 2.

Calculated voltage profiles, Pourbaix diagram and ΔG_{pbx} of $Na_3MnTi(PO_4)_3$ cathode

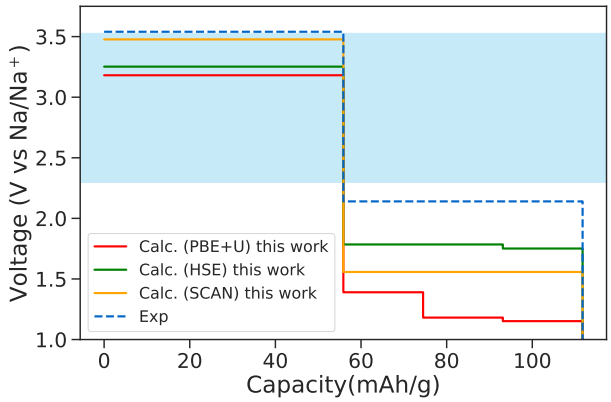

(a)

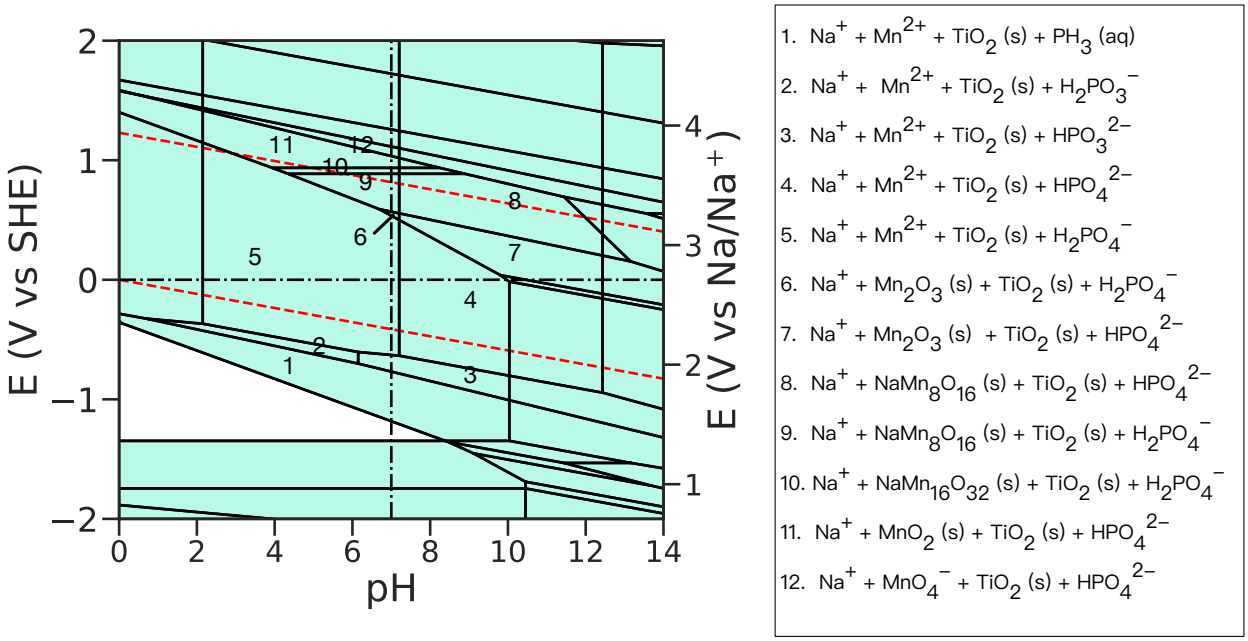

(b)

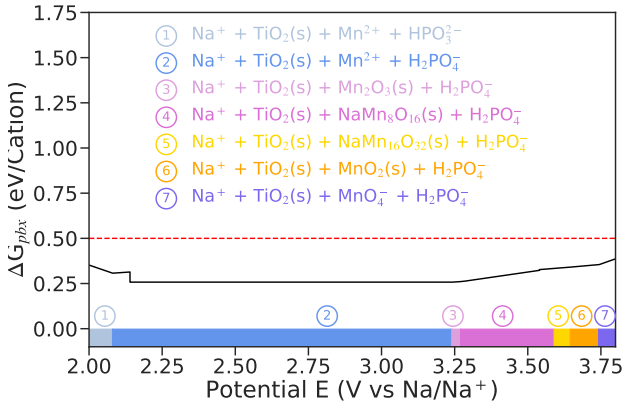

(c)

Figure S3: (a) Voltage profile of $Na_xMnTiP_3O_{12}$. Electrochemical window (pH = 7) is shaded with blue color. (b) Calculated Pourbaix diagram of $Na_3MnTiP_3O_{12}$. Regions containing solid phases are shaded with green color. (c) ΔG_{pbx} of $Na_xMnTiP_3O_{12}$ as a function of potential in neutral aqueous solution (pH = 7).

Pourbaix diagram of $Na_2FeP_2O_7$ and $Na_4Fe_3P_4O_{15}$ cathode

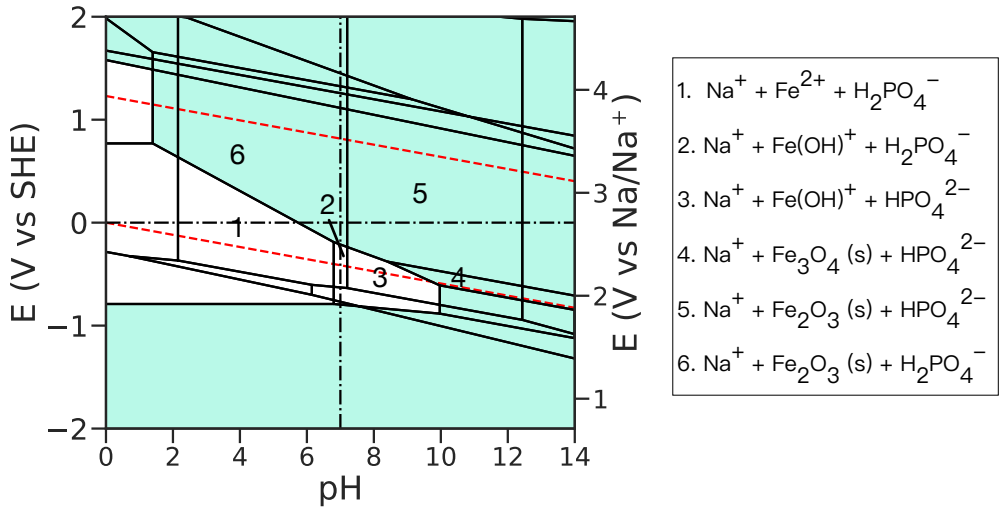

(a) Calculated Pourbaix diagram of $Na_2FeP_2O_7$

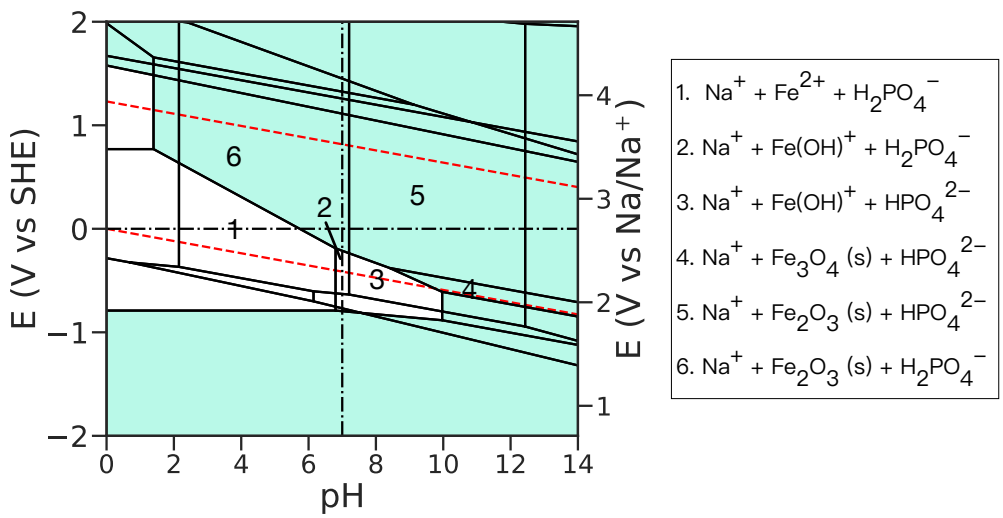

(b) Calculated Pourbaix diagram of $Na_4Fe_3P_4O_{15}$

Figure S4: Calculated Pourbaix diagram of (a) $Na_2FeP_2O_7$ and (b) $Na_4Fe_3P_4O_{15}$. Regions containing solid phases are shaded green.

Calculated ΔG_{pbx} as a function of pH of selected cathodes at their average voltage

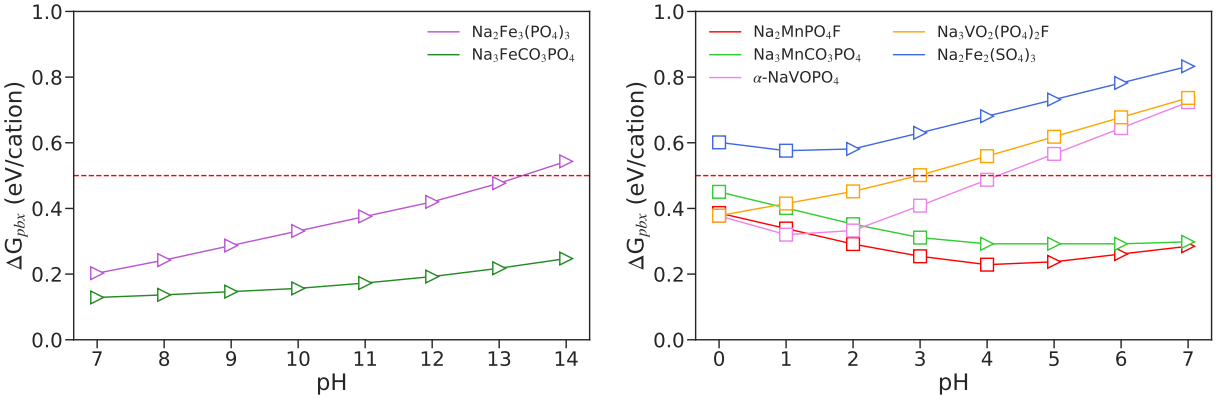

(a) (b)

Figure S5: Calculated ΔG_{pbx} vs pH of selected cathodes in (a) basic electrolytes (pH = 7 $\sim$ 14) (b) acidic electrolytes (pH = 0 $\sim$ 7). Triangle markers indicate the solid phases in decomposition products with H_2O, while square markers indicate non-solid phases in decomposition products.

Aqueous stability analysis of Na_2MnPO_4F

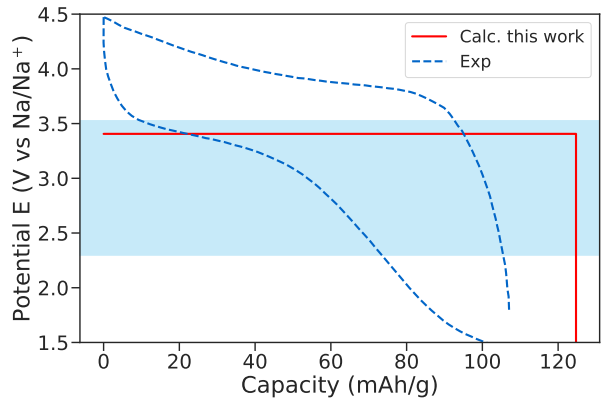

(a) Voltage profile of Na_xMnPO_4F

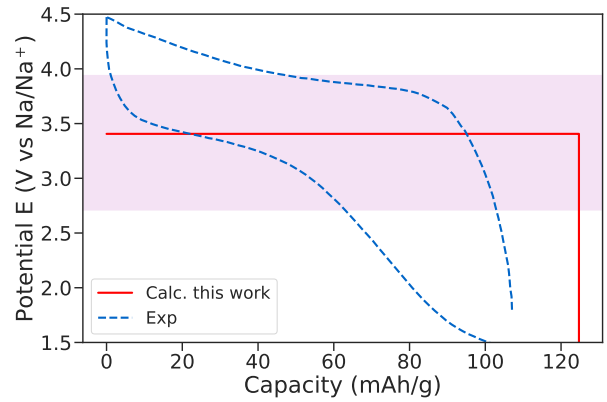

(b) Voltage profile of Na_xMnPO_4F

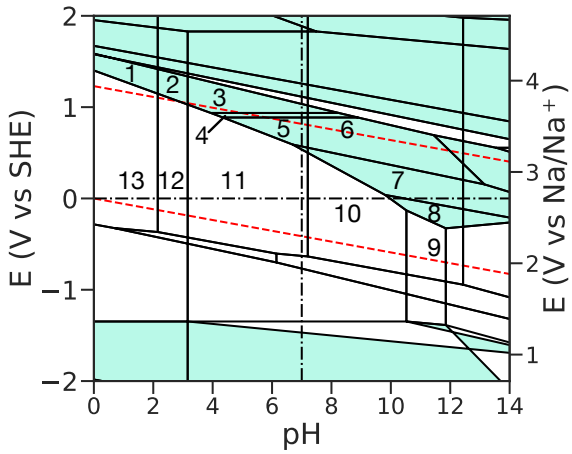

1. $Na^+ + MnO_2$ (s) + H_3PO_4 (aq) + HF (aq)
2. $Na^+ + MnO_2$ (s) + $H_2PO_4^-$ + HF (aq)
3. $Na^+ + MnO_2$ (s) + $H_2PO_4^- + F_2^{2-}$
4. $Na^+ + NaMn_{16}O_{32}$(s) + $HPO_4^{2-} + F_2^{2-}$
5. $Na^+ + NaMn_8O_{16}$ (s) + $H_2PO_4^- + F_2^{2-}$
6. $Na^+ + NaMn_8O_{16}$ (s) + $HPO_4^{2-} + F_2^{2-}$
7. $Na^+ + Mn_2O_3$ (s) + $HPO_4^{2-} + F_2^{2-}$
8. $Na^+ + Mn_3O_4$ (s) + $HPO_4^{2-} + F_2^{2-}$
9. $Na^+ + Mn(OH)^+ + HPO_4^{2-} + F_2^{2-}$
10. $Na^+ + Mn^{2+} + HPO_4^{2-} + F_2^{2-}$
11. $Na^+ + Mn^{2+} + H_2PO_4^- + F_2^{2-}$
12. $Na^+ + Mn^{2+} + H_2PO_4^-$ + HF (aq)
13. $Na^+ + Mn^{2+} + H_3PO_4$ (aq) + HF (aq)

(c) Calculated Pourbaix diagram of Na_2MnPO_4F

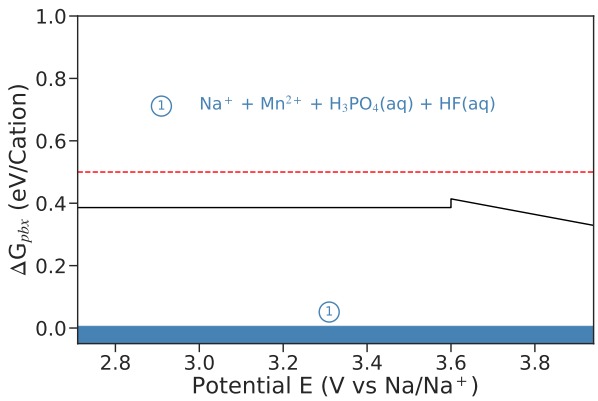

(d) ΔG_{pbx} vs E of Na_xMnPO_4F

Figure S6: Voltage profile of Na_xMnPO_4F. Electrochemical window at (a) pH =7 and (b) pH = 0 is shaded with blue and pink color, respectively. The experimental voltage profile is from ref 11 (b) Calculated Pourbaix diagram of Na_2MnPO_4F. Regions containing solid phases are shaded with green color; (c) ΔG_{pbx} of Na_xMnPO_4F as a function of potential in acidic aqueous solution (pH = 0).

Detailed calculations of the selected promising candidates as cathodes in ASIBs

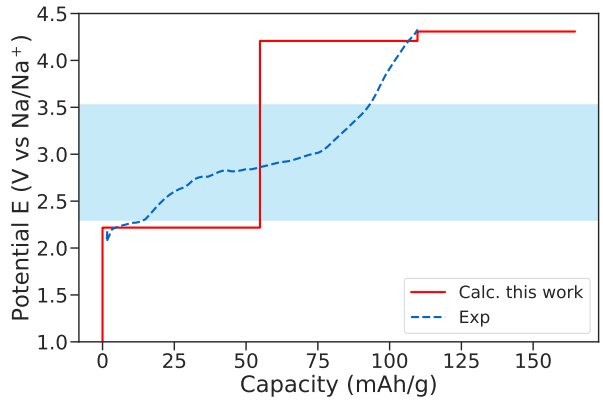

(a) Voltage profile of $Na_xFe_2(PO_4)_3$

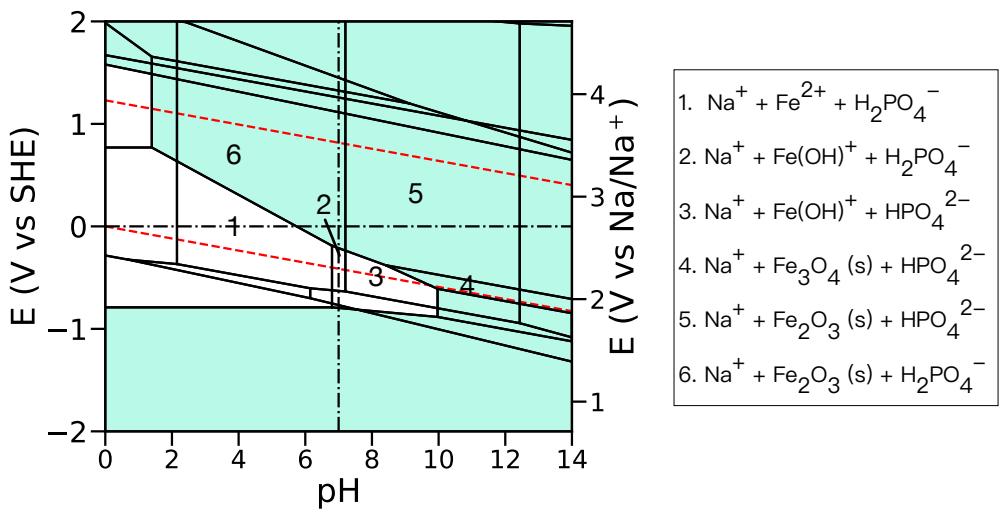

(b) Calculated Pourbaix diagram of $Na_3Fe_2(PO_4)_3$

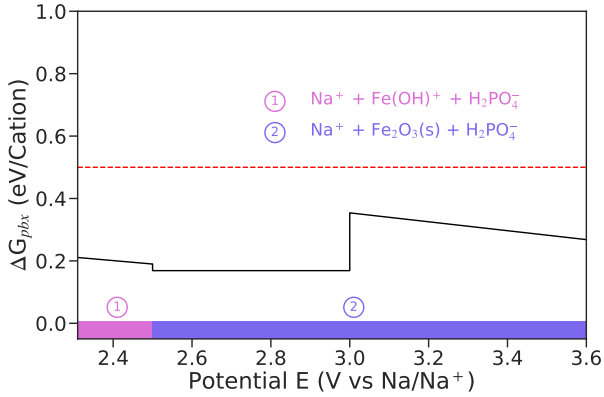

(c) ΔG_{pbx} vs E of $Na_xFe_2(PO_4)_3$

Figure S7: (a) Voltage profile of $Na_xFe_2(PO_4)_3$. Electrochemical window (pH = 7) is shaded with blue color. The experimental voltage profile is from ref 12 (b) Calculated Pourbaix diagram of $Na_3Fe_2(PO_4)_3$. Regions containing solid phases are shaded with green color. (c) ΔG_{pbx} of $Na_xFe_2(PO_4)_3$ as a function of potential in neutral aqueous solution (pH = 7).

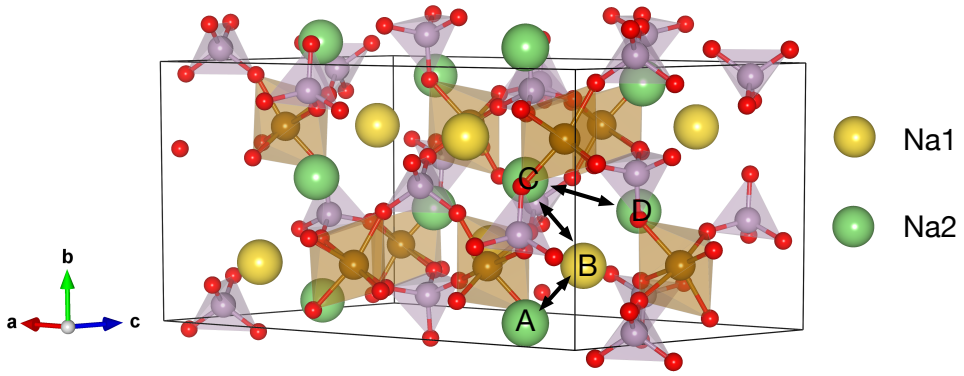

(a) Migration path

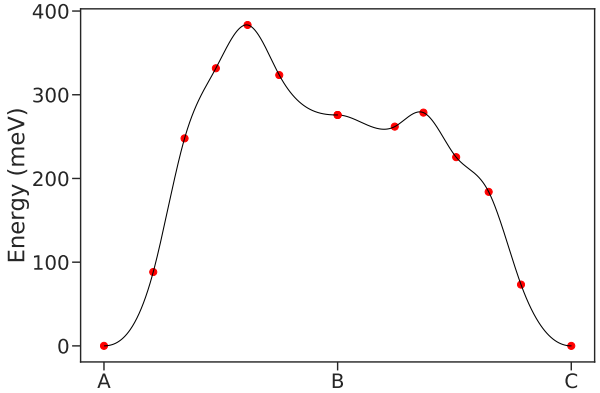

(b) A → B → C

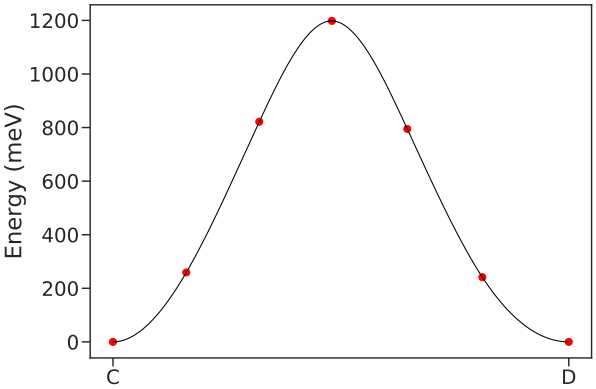

(c) C → D

Figure S8: (a) Investigated Na vacancy diffusion paths in $Na_3Fe_2(PO_4)_3$. Symmetrically distinct Na1 and Na2 are represented by green and yellow spheres, respectively. Purple tetrahedra and brown octahedra indicate PO_4 and FeO_6. (b)(c) Calculated CI-NEB migration barriers for selected percolating path.

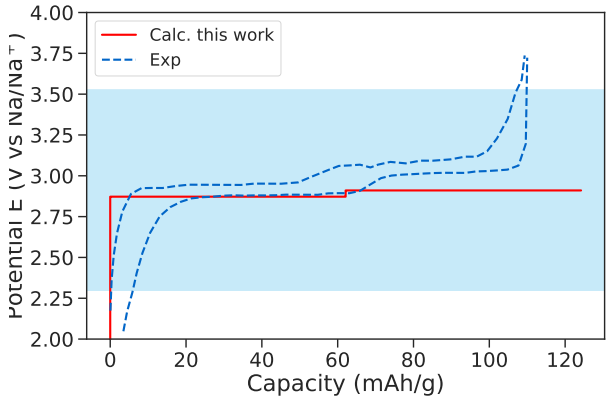

(a) Voltage profile of Na_xFePO_4F

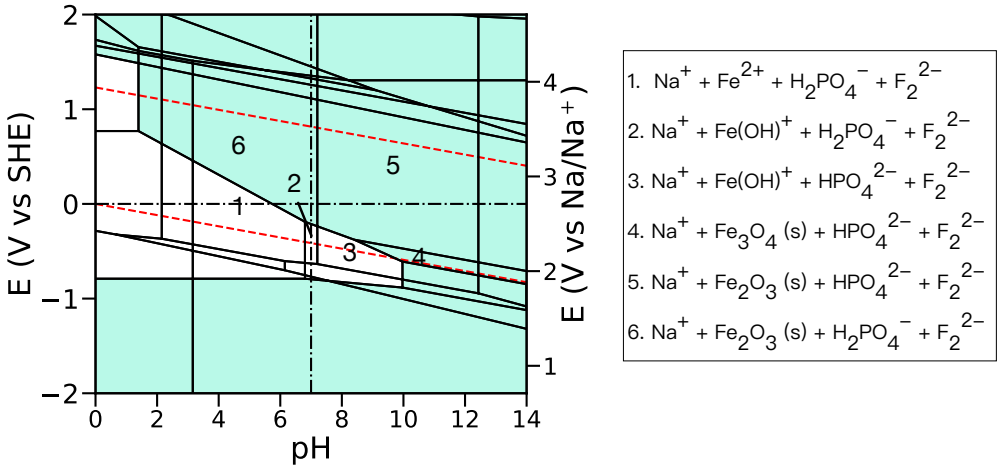

(b) Calculated Pourbaix diagram of Na_2FePO_4F

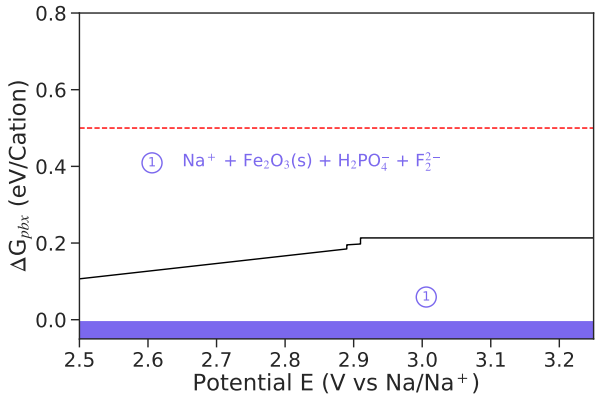

(c) ΔG_{pbx} vs E of Na_xFePO_4F

Figure S9: (a) Voltage profile of Na_2FePO_4F. Electrochemical window (pH = 7) is shaded with blue color. The experimental voltage profile is from ref 13. (b) Calculated Pourbaix diagram of Na_2FePO_4F. Regions containing solid phases are shaded with green color. (c) ΔG_{pbx} of Na_xFePO_4F as a function of potential in neutral aqueous solution (pH = 7).

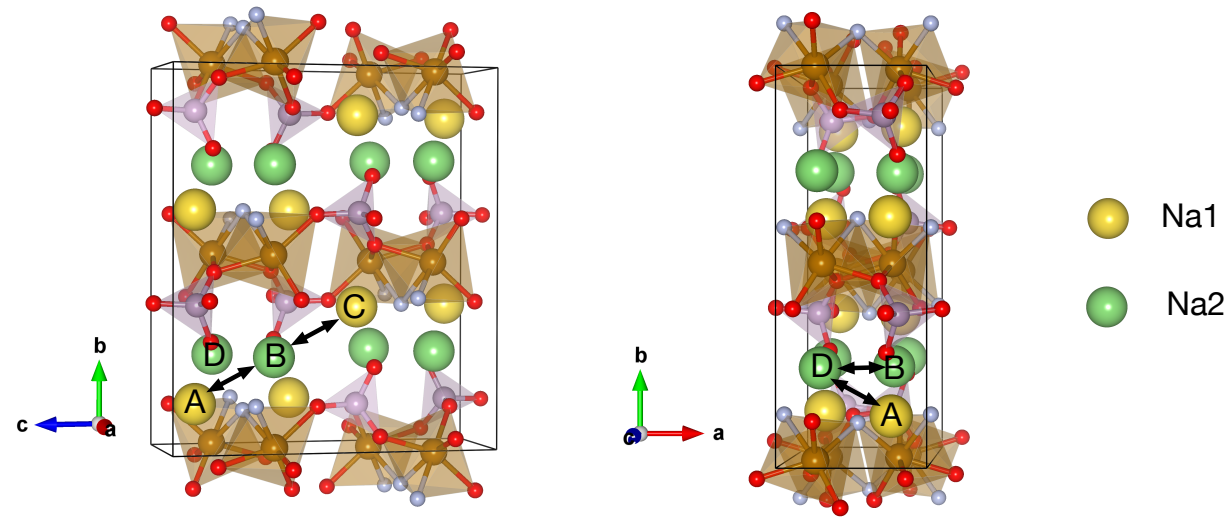

(a) Migration path

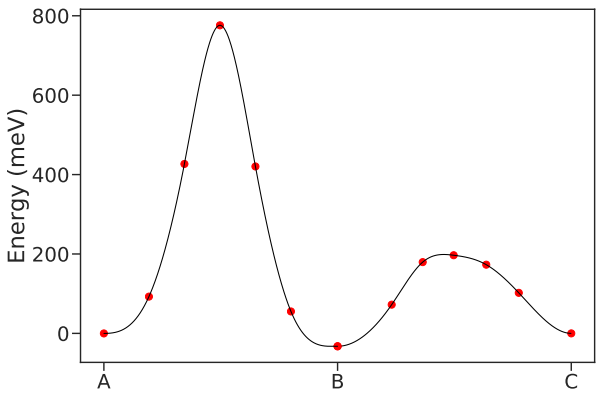

(b) A → B → C

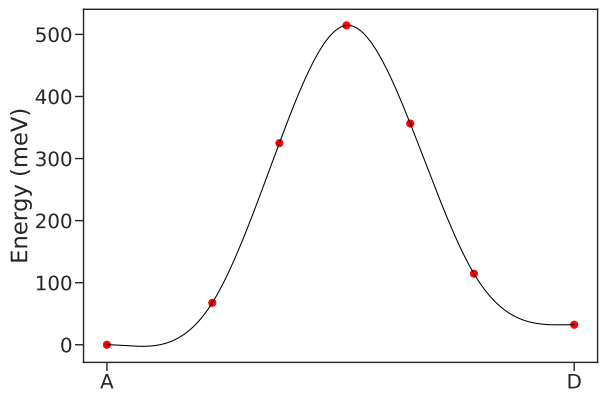

(c) A → D

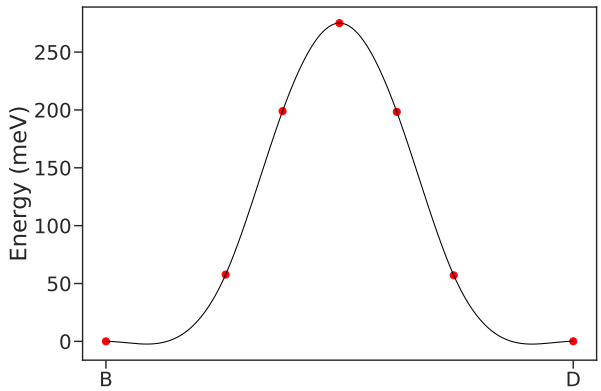

(d) B → D

Figure S10: (a) Investigated Na vacancy diffusion paths in Na_2FePO_4F. Symmetrically distinct Na1 and Na2 are represented by green and yellow spheres, respectively. Purple tetrahedra and brown octahedra indicate PO_4 and FeO_4F_2. (b)(c)(d) Calculated CI-NEB migration barriers for selected percolating path.

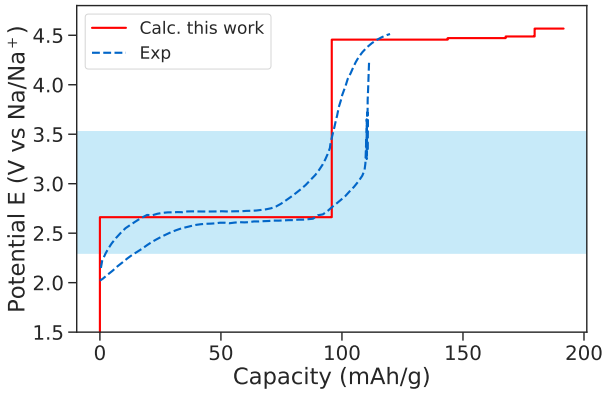

(a) Voltage profile of $Na_xFeCO_3PO_4$

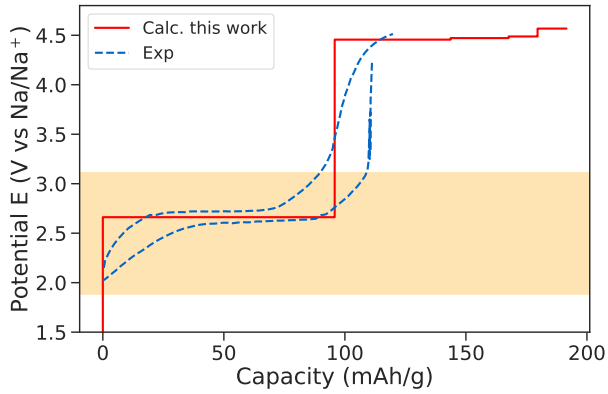

(b) Voltage profile of $Na_xFeCO_3PO_4$

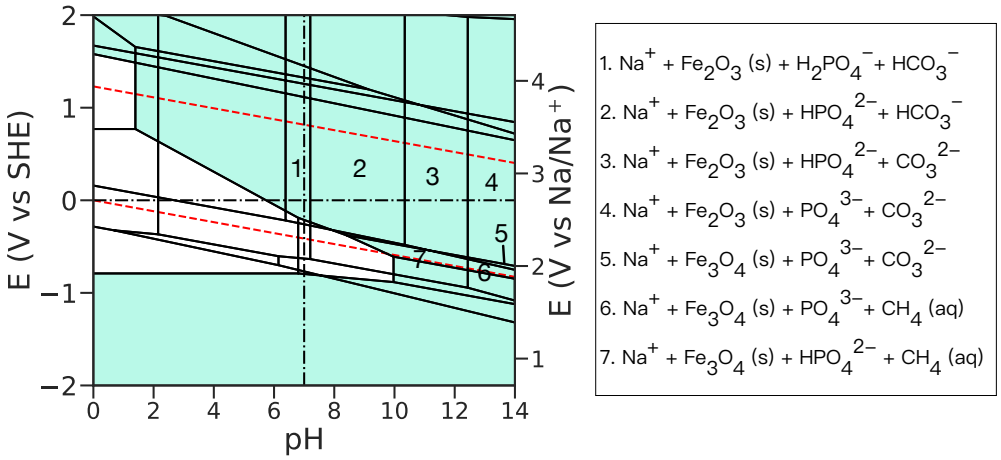

(c) Calculated Pourbaix diagram of $Na_3FeCO_3PO_4$

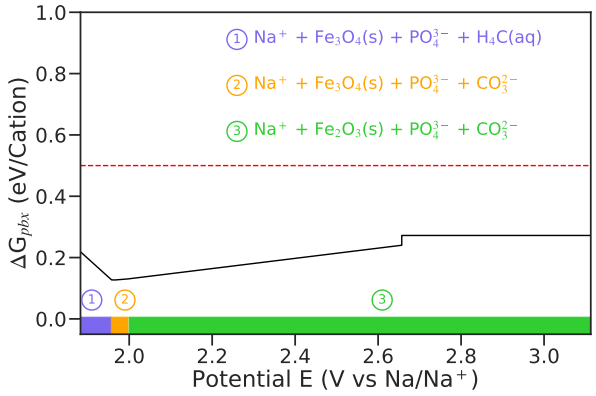

(d) ΔG_{pbx} vs E of $Na_xFeCO_3PO_4$

Figure S11: (a) Voltage profile of $Na_xFeCO_3PO_4$. Electrochemical window at pH =7 and pH = 14 is shaded with blue and orange color, respectively. The experimental voltage profile is from ref 14 (b) Calculated Pourbaix diagram of $Na_3FeCO_3PO_4$. Regions containing solid phases are shaded with green color. (c) ΔG_{pbx} of $Na_xFeCO_3PO_4$ as a function of potential in basic aqueous solution (pH = 12).

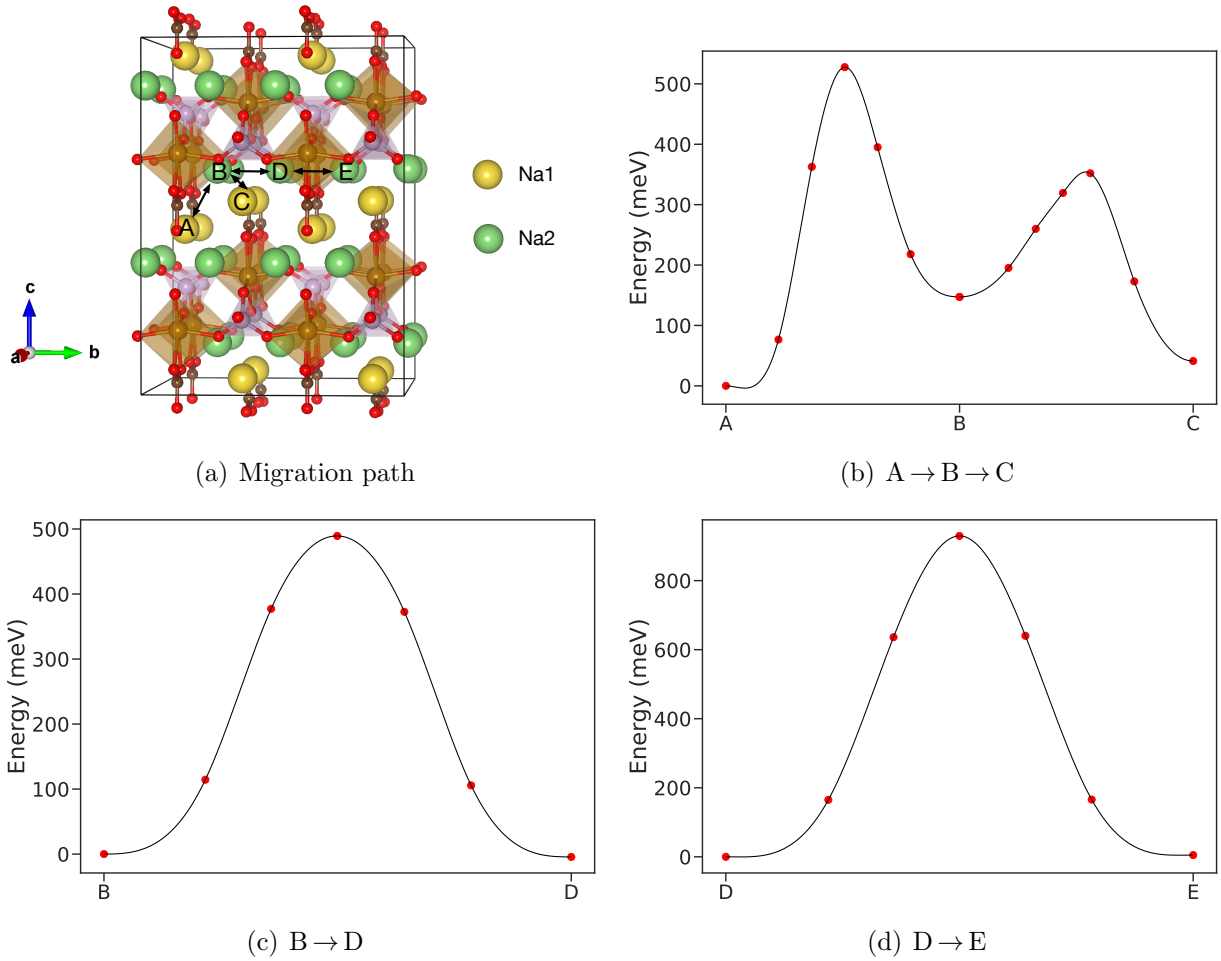

(a) Migration path

(b) A → B → C

(c) B → D

(d) D → E

Figure S12: (a) Investigated Na vacancy diffusion paths in $Na_3FeCO_3PO_4$. Symmetrically distinct Na1 and Na2 are represented by green and yellow spheres, respectively. Purple tetrahedra and brown octahedra indicate PO_4 and FeO_6. (b)(c)(d) Calculated CI-NEB migration barriers for selected percolating path.

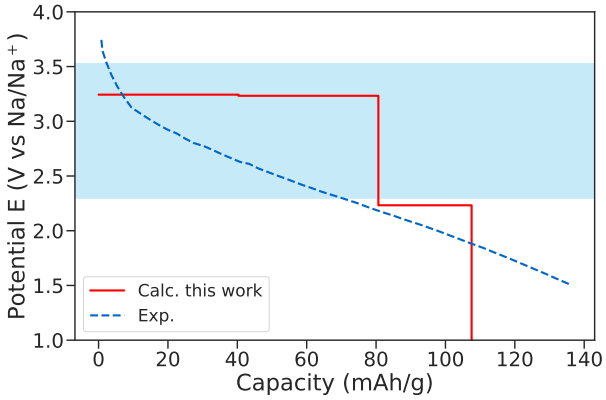

(a) Voltage profile of $Na_xFe_3(PO_4)_3$

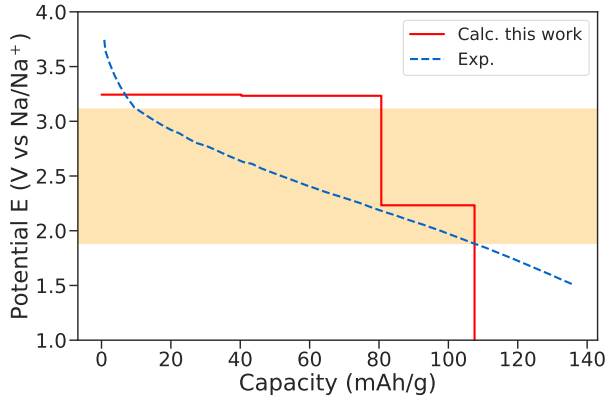

(b) Voltage profile of $Na_xFe_3(PO_4)_3$

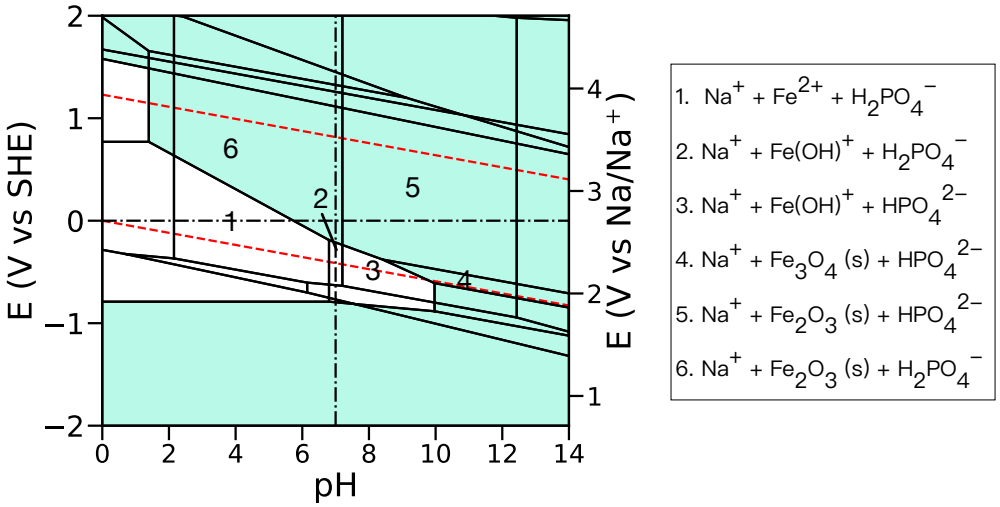

(c) Calculated Pourbaix diagram of $Na_2Fe_3(PO_4)_3$

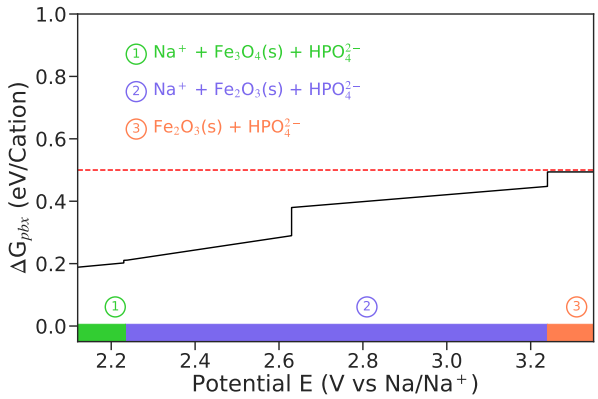

(d) ΔG_{pbx} vs E of $Na_xFe_3(PO_4)_3$

Figure S13: Voltage profile of $Na_xFe_3(PO_4)_3$. Electrochemical window at (a) pH =7 and (b) pH = 14 is shaded with blue and orange color, respectively. The experimental voltage profile is from ref 15. (b) Calculated Pourbaix diagram of $Na_2Fe_3(PO_4)_3$. Regions containing solid phases are shaded with green color. (c) ΔG_{pbx} of $Na_xFe_3(PO_4)_3$ as a function of potential in basic aqueous solution (pH = 14).

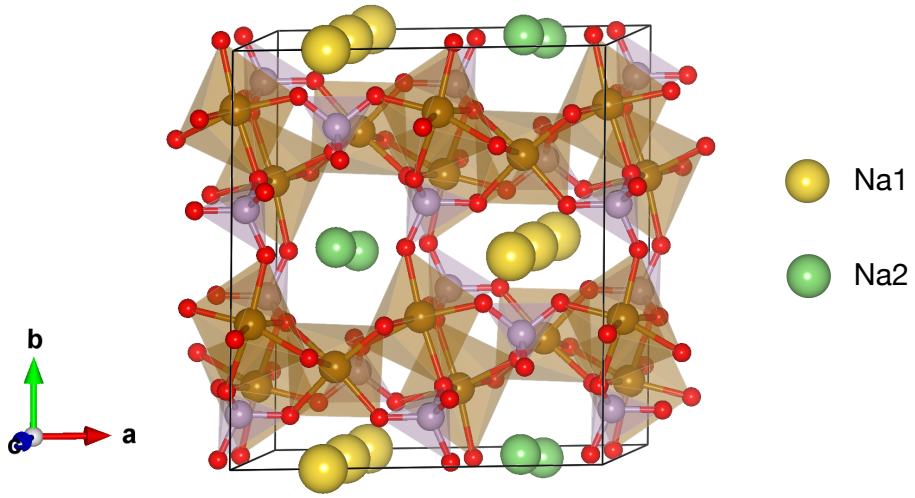

(a) Migration path

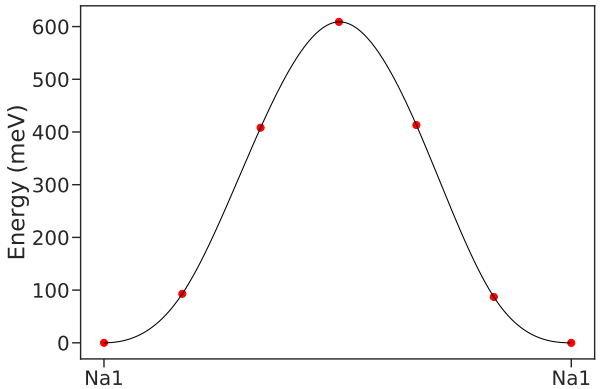

(b) Na1 → Na1

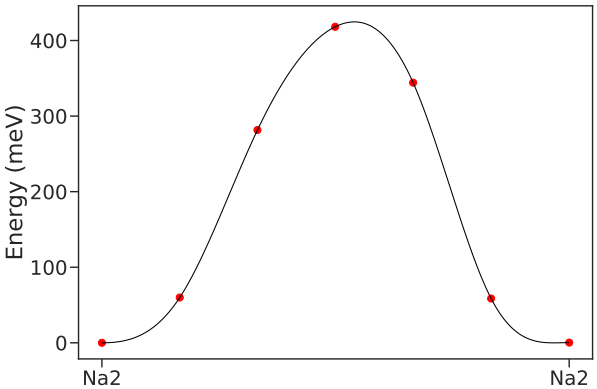

(c) Na2 → Na2

Figure S14: (a) Investigated Na vacancy diffusion paths in $Na_2Fe_3(PO_4)_3$. Symmetrically distinct Na1 and Na2 are represented by green and yellow spheres, respectively. Purple tetrahedra and brown octahedra indicate PO_4 and FeO_6. (b)(c) Calculated CI-NEB migration barriers for selected percolating path.

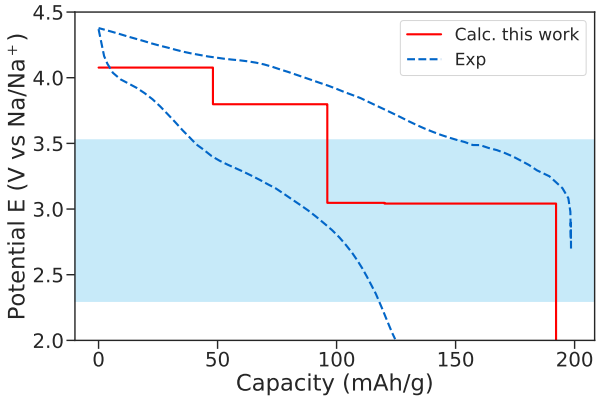

(a) Voltage profile of $Na_xMnCO_3PO_4$

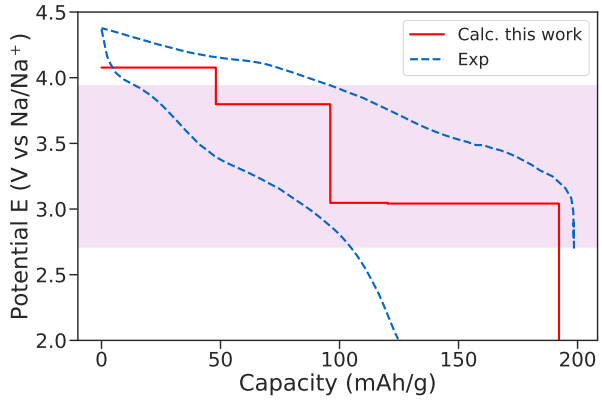

(b) Voltage profile of $Na_xMnCO_3PO_4$

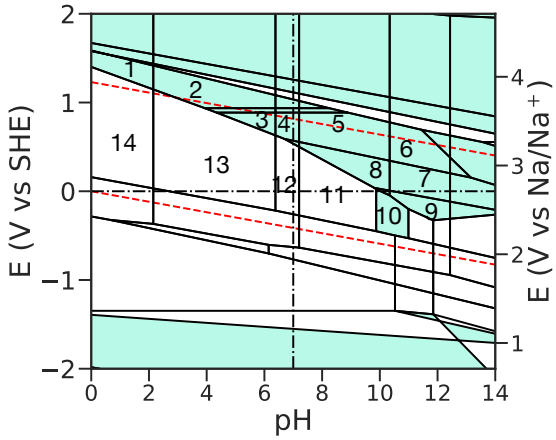

1. $Na^+ + MnO_2$ (s) + H_3PO_4 (aq) + CO_2 (aq)
2. $Na^+ + MnO_2$ (s) + $H_2PO_4^-$ + CO_2 (aq)
3. $Na^+ + NaMn_8O_{16}$ (s) + $H_2PO_4^-$ + CO_2 (aq)
4. $Na^+ + NaMn_8O_{16}$ (s) + $H_2PO_4^-$ + HCO_3^-
5. $Na^+ + NaMn_8O_{16}$ (s) + HPO_4^{2-} + HCO_3^-
6. $Na^+ + NaMn_8O_{16}$ (s) + HPO_4^{2-} + CO_3^{2-}
7. $Na^+ + Mn_2O_3$ (s) + HPO_4^{2-} + CO_3^{2-}
8. $Na^+ + Mn_2O_3$ (s) + HPO_4^{2-} + HCO_3^-
9. $Na^+ + Mn_3O_4$ (s) + HPO_4^{2-} + CO_3^{2-}
10. $Na^+ + MnCO_3$ (s)+ HPO_4^{2-}
11. $Na^+ + Mn^{2+} + HPO_4^{2-} + HCO_3^-$
12. $Na^+ + Mn^{2+} + H_2PO_3^- + CH_4$ (aq)
13. $Na^+ + Mn^{2+} + H_2PO_4^- + CO_2$ (aq)
14. $Na^+ + Mn^{2+} + H_3PO_4$ (aq) + CO_2 (aq)

(c) Calculated Pourbaix diagram of $Na_3MnCO_3PO_4$

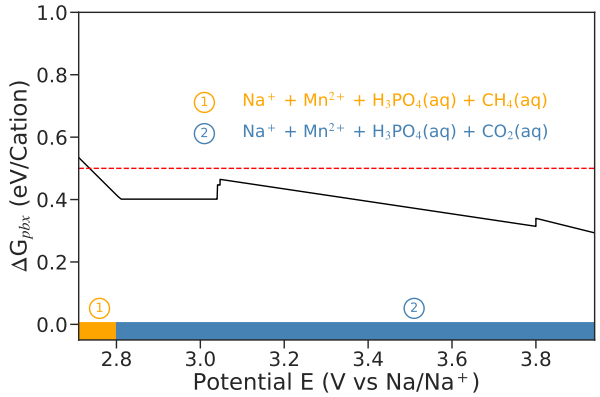

(d) ΔG_{pbx} vs E of $Na_xMnCO_3PO_4$ at pH = 1

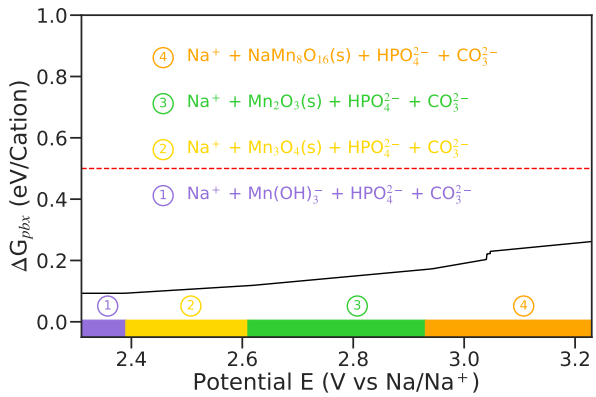

(e) ΔG_{pbx} vs E of $Na_xMnCO_3PO_4$ at pH = 12

Figure S15: Voltage profile of $Na_xMnCO_3PO_4$. Electrochemical window at (a) pH =7 and (b) pH = 0 is shaded with blue and pink color, respectively. The experimental voltage profile is from ref 16. (b) Calculated Pourbaix diagram of $Na_3MnCO_3PO_4$. Regions containing solid phases are shaded with green color. ΔG_{pbx} of $Na_xMnCO_3PO_4$ as a function of potential (c) in acidic aqueous solution (pH = 1)and (d)in basic aqueous solution (pH = 12).

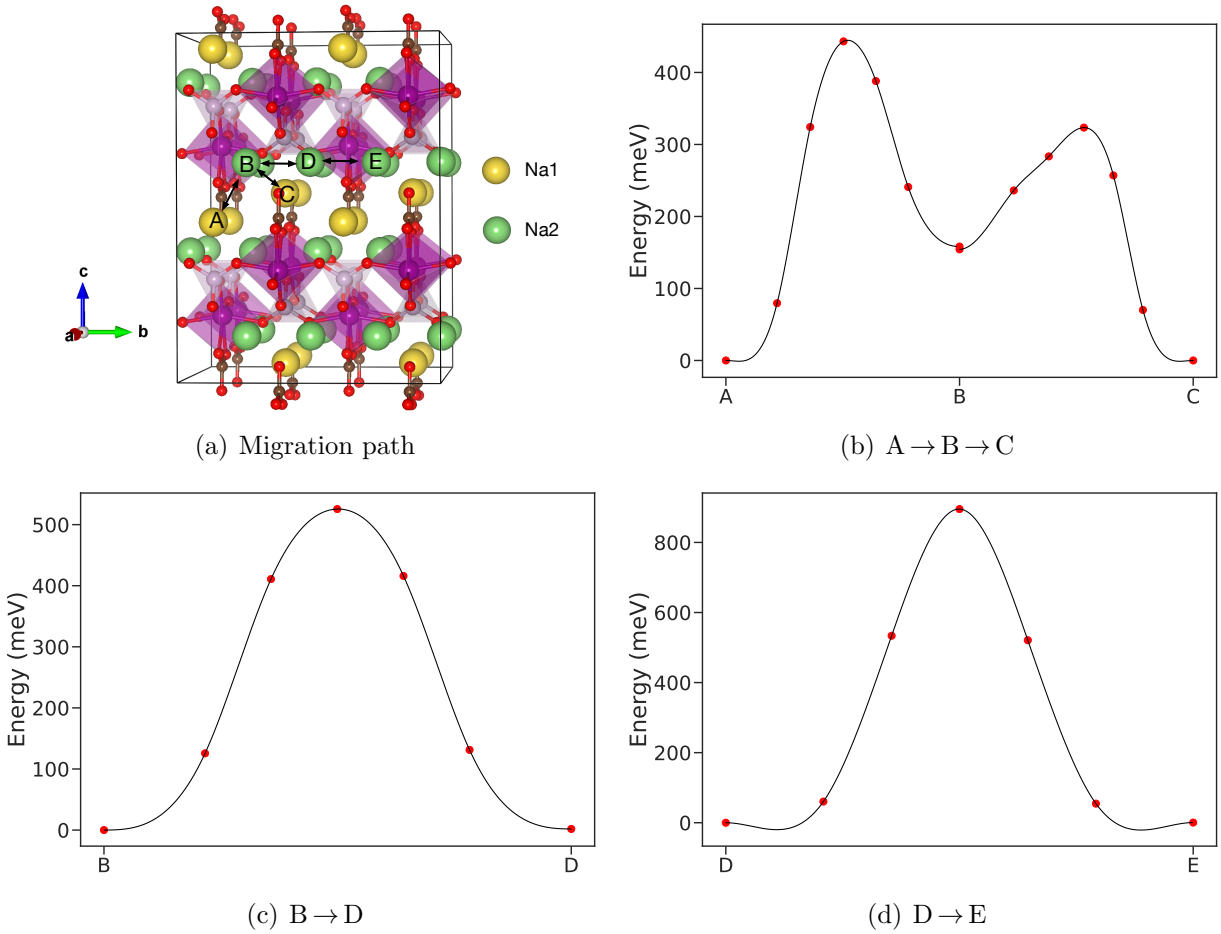

(a) Migration path

(b) A → B → C

(c) B → D

(d) D → E

Figure S16: (a) Investigated Na vacancy diffusion paths in $Na_3MnCO_3PO_4$. Symmetrically distinct Na1 and Na2 are represented by green and yellow spheres, respectively. Purple tetrahedra and violet octahedra indicate PO_4 and MnO_6. (b)(c)(d) Calculated CI-NEB migration barriers for selected percolating path.

References

(1) Cao, Y.; Xiao, L.; Wang, W.; Choi, D.; Nie, Z.; Yu, J.; Saraf, L. V.; Yang, Z.; Liu, J. Reversible sodium ion insertion in single crystalline manganese oxide nanowires with long cycle life. *Advanced Materials* **2011**, *23*, 3155–3160.

(2) Kim, H.; Kim, D. J.; Seo, D.-H.; Yeom, M. S.; Kang, K.; Kim, D. K.; Jung, Y. Ab initio study of the sodium intercalation and intermediate phases in $Na_{0.44}MnO_2$ for sodium-ion battery. *Chemistry of Materials* **2012**, *24*, 1205–1211.

(3) Saravanan, K.; Mason, C. W.; Rudola, A.; Wong, K. H.; Balaya, P. The first report on excellent cycling stability and superior rate capability of $Na_3V_2(PO_4)_3$ for sodium ion batteries. *Advanced Energy Materials* **2013**, *3*, 444–450.

(4) Lim, S. Y.; Kim, H.; Shakoor, R.; Jung, Y.; Choi, J. W. Electrochemical and thermal properties of NASICON structured Na_3V_2 $(PO_4)_3$ as a sodium rechargeable battery cathode: a combined experimental and theoretical study. *Journal of The Electrochemical Society* **2012**, *159*, A1393.

(5) Kim, H.; Shakoor, R.; Park, C.; Lim, S. Y.; Kim, J.-S.; Jo, Y. N.; Cho, W.; Miyasaka, K.; Kahraman, R.; Jung, Y., et al. $Na_2FeP_2O_7$ as a promising iron-based pyrophosphate cathode for sodium rechargeable batteries: a combined experimental and theoretical study. *Advanced Functional Materials* **2013**, *23*, 1147–1155.

(6) Boucher, F.; Gaubicher, J.; Cuisinier, M.; Guyomard, D.; Moreau, P. Elucidation of the $Na_{2/3}FePO_4$ and $Li_{2/3}FePO_4$ intermediate superstructure revealing a pseudouniform ordering in 2D. *Journal of the American Chemical Society* **2014**, *136*, 9144–9157.

(7) Saracibar, A.; Carrasco, J.; Saurel, D.; Galceran, M.; Acebedo, B.; Anne, H.; Lepoitevin, M.; Rojo, T.; Cabanas, M. C. Investigation of sodium insertion–extraction in olivine Na_xFePO_4 ($0 \leq x \leq 1$) using first-principles calculations. *Physical Chemistry Chemical Physics* **2016**, *18*, 13045–13051.

(8) Oh, S.-M.; Myung, S.-T.; Hassoun, J.; Scrosati, B.; Sun, Y.-K. Reversible $NaFePO_4$ electrode for sodium secondary batteries. *Electrochemistry Communications* **2012**, *22*, 149–152.

(9) Li, Q.; Liu, Z.; Zheng, F.; Liu, R.; Lee, J.; Xu, G.-L.; Zhong, G.; Hou, X.; Fu, R.; Chen, Z., et al. Identifying the structural evolution of the sodium ion battery Na_2FePO_4F cathode. *Angewandte Chemie* **2018**, *130*, 12094–12099.

(10) Shinagawa, C.; Morikawa, Y.; Nishimura, S.-i.; Ushiyama, H.; Yamada, A.; Yamashita, K. A Theoretical study on the charge and discharge states of Na-ion battery cathode material, $Na_{1+x}FePO_4F$. *Journal of computational chemistry* **2019**, *40*, 237–246.

(11) Jung, Y. H.; Lim, C. H.; Kim, J.-H.; Kim, D. K. $Na_2FeP_2O_7$ as a positive electrode material for rechargeable aqueous sodium-ion batteries. *Rsc Advances* **2014**, *4*, 9799–9802.

(12) Rajagopalan, R.; Chen, B.; Zhang, Z.; Wu, X.-L.; Du, Y.; Huang, Y.; Li, B.; Zong, Y.; Wang, J.; Nam, G.-H., et al. Improved reversibility of Fe^{3+}/Fe^{4+} redox couple in sodium super ion conductor type $Na_3Fe_2(PO_4)_3$ for sodium-ion batteries. *Advanced Materials* **2017**, *29*, 1605694.

(13) Kawabe, Y.; Yabuuchi, N.; Kajiyama, M.; Fukuhara, N.; Inamasu, T.; Okuyama, R.; Nakai, I.; Komaba, S. Synthesis and electrode performance of carbon coated Na_2FePO_4F for rechargeable Na batteries. *Electrochemistry Communications* **2011**, *13*, 1225–1228.

(14) Huang, W.; Zhou, J.; Li, B.; Ma, J.; Tao, S.; Xia, D.; Chu, W.; Wu, Z. Detailed investigation of $Na_{2.24}FePO_4CO_3$ as a cathode material for Na-ion batteries. *Scientific reports* **2014**, *4*, 4188.

(15) Huang, W.; Li, B.; Saleem, M. F.; Wu, X.; Li, J.; Lin, J.; Xia, D.; Chu, W.; Wu, Z. Self-Assembled Alluaudite $Na_2Fe_{3-x}Mn_x(PO_4)_3$ Micro/Nanocompounds for Sodium-Ion Battery Electrodes: A New Insight into Their Electronic and Geometric Structure. *Chemistry–A European Journal* **2015**, *21*, 851–860.

(16) Chen, H.; Hao, Q.; Zivkovic, O.; Hautier, G.; Du, L.-S.; Tang, Y.; Hu, Y.-Y.; Ma, X.; Grey, C. P.; Ceder, G. Sidorenkite ($Na_3MnPO_4CO_3$): a new intercalation cathode material for Na-ion batteries. *Chemistry of Materials* **2013**, *25*, 2777–2786.